A new correlation technique for ice-motion analysis

Yan Sun

Department of Radio and Space Science
Chalmers University of Technology
S-412 96 Göteborg, Sweden

ABSTRACT

Several algorithms for extracting ice motion information from satellite images have been developed since late 1980's. The motion measurements are generally made by matching individual features (e.g. floes and boundaries etc.). Instead, we derive motion vectors by matching the entire images to each other. Such a match is possible in the centre of the pack ice area, since internal movements of the ice packs are much smaller than the image size within an image scene. The method used is simply a matter of finding the maximum in the cross correlation function of two images. However, the existence of a rotation between the two images causes the peak to vanish. In this paper we introduce a polar co-ordinate system to present the power spectra of images by which the rotation angle can easily be detected. After removing the relative rotation, the vanishing peak will show up. This new correlation algorithm has been applied to 19 image pairs acquired during the ARCTIC-91 expedition and is successful for most of the image pairs. The ice motion measurements have been compared with the wind speeds to study the relation between the velocities of ice motion and wind.

1. INTRODUCTION

The automatic sea ice tracking technique has shown great promise in monitoring the dynamics of sea ice since late 1980's. There are several approaches which are based on different similarity measurements to match individual features, such as matching corresponding sub-scenes of two images by their correlation coefficients, (Fily and Rothrock 1987, Vesecky et al. 1987), matching edges in terms of the deviations in floe-lead boundaries from straight-line segments (Vesecky et al. 1988) and identifying floes by Ψ-S curves of their shapes (McConnell et al. 1991), or by a stochastic approach (Banfield 1991). In this paper we developed an algorithm which use Fourier technique to match the entire scene of images. The basic reason that such match is possible is that within an image scene the internal movements of ice packs are several kilometres which are much less than the image size (100 km). Therefore, the internal movements are negligible for an image with a large pixel spacing (e.g. 400 m). From this the assumption naturally arises that large ice packs have rigid motion (i.e. translation and rotation). The simplest way to determine a translation is to use the cross-correlation technique which is just a matter of finding the location of the peak in a cross-correlation function. However, the method is very sensitive to a rotation between two images. A rotation of only a few degree will cause the peak vanish (Castro and Morandi 1987, and Lee et al. 1988).

Several authors presented algorithms to deal with the rotational translation based on the property of the Fourier transformation. Castro and Morandi (1987) introduced the function $G(u, v, \theta)$ which is a ratio of the Fourier transforms of two images, and the rotation angle is determined by varying θ until the inverse Fourier transforms of $G(u, v, \theta)$ gives the closest shape of an unity pulse. Similarly, (Lee et al. 1988) defined another function $D(\theta)$ which is the sum of the difference between the power spectra of images, and a search strategy is used to obtain the rotation angle which results in $D(\theta)$ being close to zero. The drawback of these algorithms is that they require a search procedure which is time consuming and they are not robust, because the initial guess of θ and the search step should be carefully constructed to obtain a certain accuracy.

To avoid such a search procedure we introduce the polar co-ordinates to present power spectra. In the new co-ordinates the rotation parameter θ_0 becomes a translation parameter so that the cross-correlation technique can be applied on the transformed power spectra to obtain the rotation angle. The efficiency of such transformation will be evi-

dent by the example in section 4. Although there is a large rotation (44°) and only a small overlap (one third of the entire scene) between two images, the peaks are clearly seen in the cross-correlation functions for both the power spectra and the spatial intensities.

2. THEORY

The key step of our algorithm, is to transform power spectra. To explain the transformation, firstly we look at the Fourier transforms of two images.

Let $S_r(x, y)$ represent the reference image and $S_t(x, y)$ be the target image which is obtained by rotating S_r with θ_0 and translating with (x_0, y_0). In the spatial domain, the two images have a relation as follows:

$$S_t(x, y) = S_r(x', y') \tag{1}$$

where

$$x - x_0 = x'\cos\theta_0 - y'\sin\theta_0$$
$$y - y_0 = x'\sin\theta_0 + y'\cos\theta_0$$

According to the Fourier shift and rotation theorems, the Fourier transforms of the two images are related by

$$F_t(u, v) = e^{-j2\pi(ux_0 + vy_0)} F_r(u\cos\theta_0 + v\sin\theta_0, -u\sin\theta_0 + v\cos\theta_0) \tag{2}$$

and the relation between their power spectra is

$$P_t(u, v) = P_r(u', v') \tag{3}$$

where

$$u' = v\cos\theta_0 + u\sin\theta_0$$
$$v' = u\sin\theta_0 + v\cos\theta_0$$

Equation (3), indicates that: P_t and Pr are not affected by translation parameters x_0, y_0 (i.e. they are translation invariant), but only related by the rotation angle θ_0. From the relation between (u, v) and (u', v'), we introduce the polar co-ordinates, i.e.

$$r = \sqrt{u^2 + v^2} \tag{4a}$$
$$\theta = \arctan\left(\frac{v}{u}\right) \tag{4b}$$

where the r axis corresponds to frequency and has a range of 0 to 1/2 length of an image side. θ describes the direction of frequency and has a range of 0° to 360°.

Then, P_t and P_r are related by

$$P_t(r, \theta) = P_r(r, \theta + \theta_0) \tag{5}$$

As we expected, in the new co-ordinate system (r, θ) the rotation parameter becomes a translation parameter. Therefore the cross-correlation function of P_t and P_r can be calculated according to equation (6).

$$CC(\eta, \alpha) = \int_{r_1}^{r_2} \int_{\theta_1}^{\theta_2} P_t(r + \eta, \theta + \alpha)\, P_r(r, \theta)\, d\theta\, dr \tag{6}$$

where r_1, r_2, θ_1, and θ_2 are determined based on the following considerations.

Since very low frequency components are not sensitive to a small rotation and very high frequency components are mainly noise, from practical test we have chosen $r_1 = 10$ (pixel), and $r_2 = 74$ (pixel), for an image with a size of 256 x 256 (pixels). The interval (θ_1, θ_2) is chosen to be 180°, as the power spectrum is an even symmetric function.

The $CC(\eta, \alpha)$ will contain a peak whose position (η_0, α_0) indicates the rotation between P_t and P_r, i.e. $\alpha_0 = \theta_0$, and $\eta_0 = 0$ (suppose that there is no scale change between the two images).

3. IMPLEMENTATION

In order to use ordinary image processing software, the function $CC(\eta, \alpha)$ is not computed in polar co-ordinates. Instead, the integral circular area in equation (6) is projected to a rectangular one as shown in Fig. 1. Then, the cross-correlation $CC(\eta, \alpha)$ is presented in Cartesian co-ordinates as CC(p, q) where the peak position is (p_n, q_a), and θ_0 is determined by

$$\theta_0 = \frac{q_a 180}{r_2 \pi} \tag{7}$$

An image S'_t which is compensated for the rotation can, now be obtained by rotating S_t with $-\theta_0$. The translation can now be determined from the cross-correlation function of S_r and S'_t.

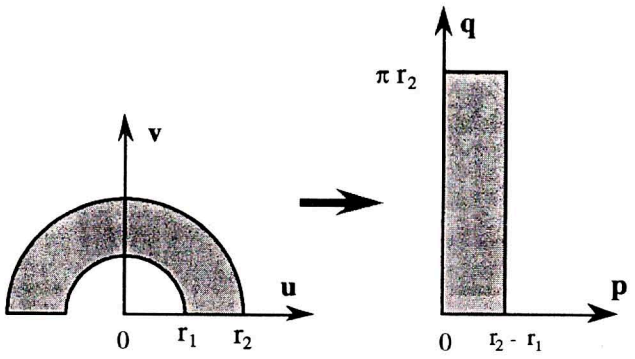

Fig. 1 - The projection for the integral circular area of equation (6)

4. EXAMPLE

Two images, S_1 and S_2, (Fig. 2a and 2b) were chosen to illustrate the method. The size of the images is 256 x 256 (pixels). S_2 is obtained from S_1 and the objects within the scene have been rotated by 44° and translated by (-78, 126). This can be verified by comparing the common image features (marked 1,2, and 3) in S_1 and S_2.

The algorithm starts by determining the rotation angle in terms of $CC(\eta, \alpha)$ function defined in equation (6). In Fig. 3 the $CC(\eta, \alpha)$ function of S_1 and S_2 is plotted in rectangular co-ordinates (cf. Fig. 1), where the peak is located at (0,57) and hence θ_0 is 44° from equation (7). This angle is, then used for orienting S_2 to yield S_2'. The cross-correlation function between S_1 and S_2' is displayed as a grey scale image (Fig. 2d), where the peak shows up as a bright dot, whose location (78, -126) indicates the translation between S_1 and S_2'.

When the parameters of rotation and translation are determined, S_2 can rotation and translation compensated (Fig. 2c) in such a way that common features in both images are located at the same co-ordinates, cf. Fig. 2a and 2c.

5. MODIFICATION

When analysing two SAR images a peak in the conventional cross-correlation function is usually not sharp enough to accurately determine its location. Thus a modification is introduced based on the fact that a cross-correlation function is obtained by applying the inverse FFT to the cross-power spectrum. Taking logarithm on the magnitude of the cross-power spectrum, while keeping its phase term, a pseudo cross-power spectrum is constructed. Then, the inverse FFT is applied on this pseudo spectrum, which will give a higher SNR (signal-to-noise ratio) than the conventional one. To illustrate this, we choose two random processes (for simplicity one dimensional signals were used) shown in Fig. 4, where the process (a) is a replica of process (b) except for a 10 pixel delay. The marked point in (a) corresponds to the start point in (b). Two kinds of cross-correlation functions of the processes are plotted in Fig. 5. and it is clear that the pseudo cross-correlation function has superior SNR properties.

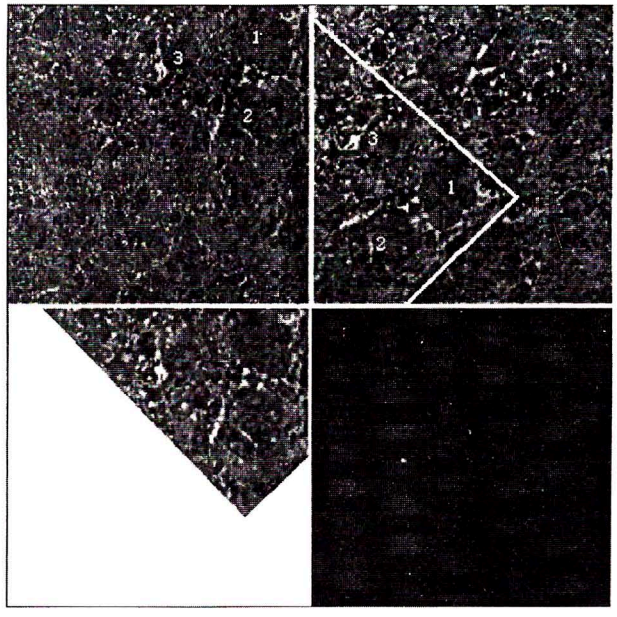

Fig. 2 - (a) the reference image, S_1 (b) the target image, S_2 Three common features are marked in S_1 ans S_2, as well as the image edge of S_1 in S_2; (c) the rotation and translation compensated image of S_2 (d) the cross-correlation function of S_1 and S_2'

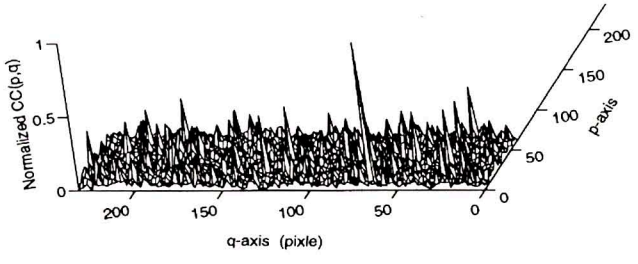

Fig. 3 - The cross-correlation functions for the power spectra

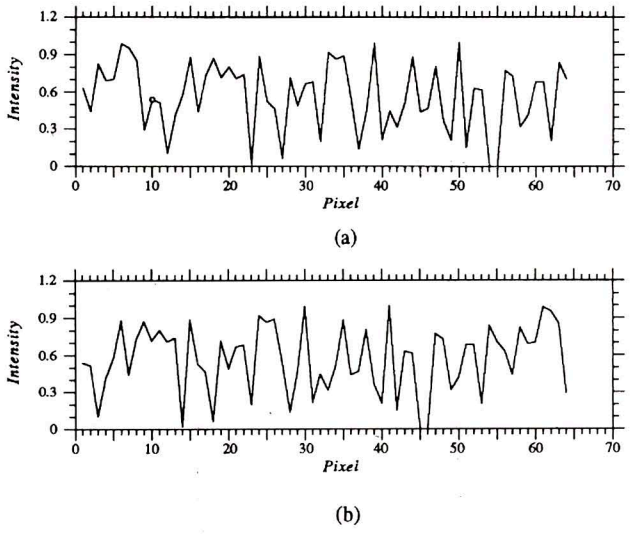

Fig. 4 - Gaussian random processes (a) and (b)

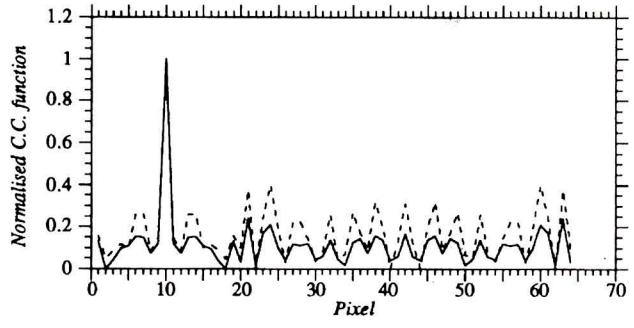

Fig. 5 - The improvement of SNR by pseudo cross-correlation function. The solid line is the pseudo cross-correlation function ans the dashed line is the conventional one

6. EXPERIMENTAL RESULTS

6.1 Data set

The data used in this paper are ERS-1 SAR images for the ARCTIC-91 expedition, acquired in the period from 17 August to 4 October, 1991. There are two kinds of products, precision (PRI) images and fast delivery (FD) images with a pixel spacing 12.5m x 12.5m and 20m x 16m respectively. The area studied lies between 10° W to 40° E, and 81° N to 84° N. The images consist of 8 frames acquired from four different orbits. Each frame covers 100 x 100 km^2. The location of these frames is shown in Fig. 6.

6.2 Results

The algorithm described in the preceding sections is applied on coarse resolution images in order to remove the small-scale deformations and to reduce computation time. Therefore, the original SAR images are averaged over 32 x 32 and 16 x 20 pixels, resulting in pixel spacing of 400 x 400 m^2 and 320 x 320 m^2 for the PRI and FD images, respectively. The averaging number for FD images is smaller than that for PRI images, due to the reduction in radiometric and spatial resolution of the former.

Most of the image pairs (17 pairs) are analysed without any problems. There are two pairs to which the cross-correlation technique is difficult to apply. One image pair is the frame 1773 acquired from orbit 955 on 21 September and from orbit 998 on 24 September. The other one is the frame 1719 acquired from orbit 941 on 20 September and from orbit 1027 on 26 September.

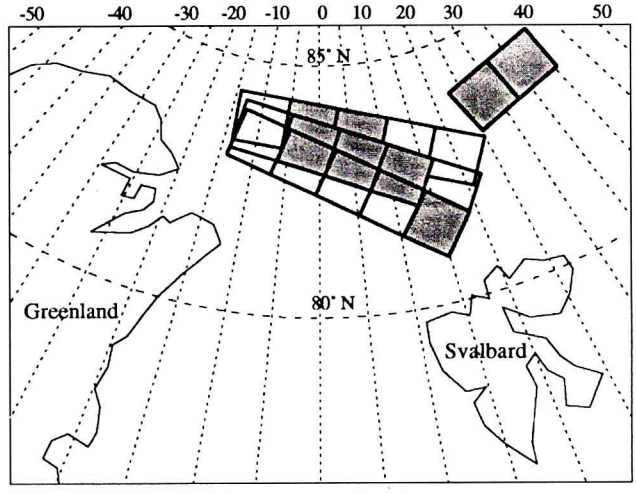

Fig. 6 - The locations of the images used for the ice motion study (shadow areas)

The main problem for the image pair in frame 1773 is that the open leads, which are usually the boundaries of ice floes, have different intensities in the two images, due to different wind conditions. Higher values are found in the image from 21 September comparing with those in the other image. This problem has been solved by substituting the highest intensity values (determined by an empirical threshold) with a low value for the image from 21 September. Fig. 7c shows the resulting image. For comparison the original image pair is shown in Fig. 7a and 7b. The other image pair (frame 1719 from orbit 941 and 1027) is more difficult to deal with by the cross-correlation technique, due to the large changes in the relative locations of ice floes and the basic assumption of mainly a translation and rotation is violated. An approximate measurement of drift is made by applying the method to a sub-scene (up-right part of the entire scene) see Fig. 8a and 8b, which is 1/4 of the entire scene having less deformation. The rest of the scene shows dramatic changes. As an example another sub-scene (down-left part of the entire scene) is also included in Fig. 8c and 8d to show the changes of the relative locations of the ice floes.

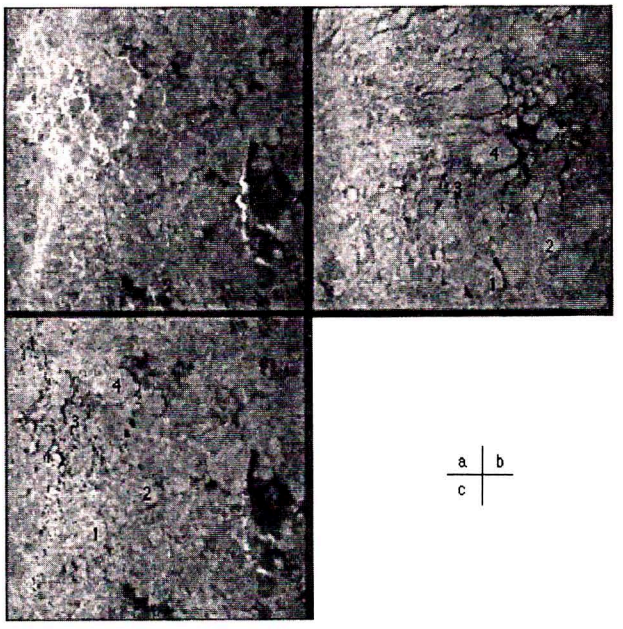

Fig. 7 - The images from frame 1773; (a) the image acquired on 21 September; (b) the image acquired on 24 September; and (c) the substituted image of image (a)

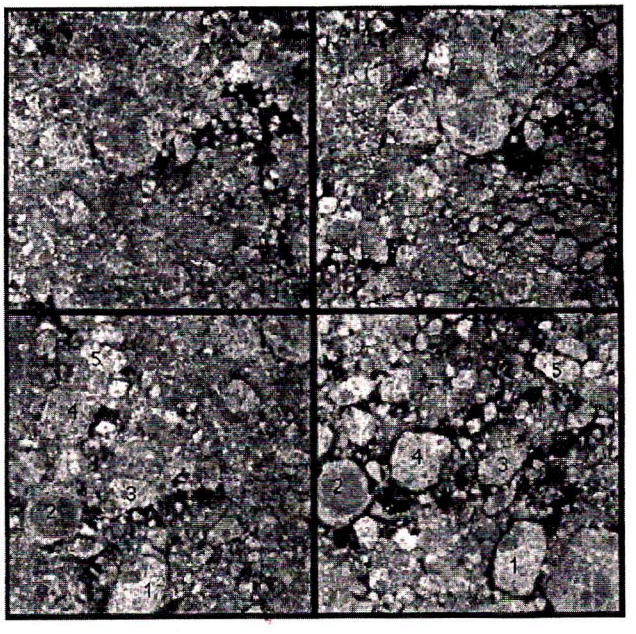

Fig. 8 - Two sub-scenes of frame 1719; (a) and (b) up-right part of the frame; (c) and (d) down-left part of the frame, where the left images are from 20 September and those on the right are from 26 September

Table 1 lists all results for the 19 image pairs, where the mean drift in all cases is less than 50 km (half-size of the ERS-1 SAR image). The results tell us that two ERS-1 SAR images, acquired at the same location within a three day period, at least have 40 percentage overlap. As manifested in section 4, our algorithm is able to deal with a pair of images which have only one third of overlap. Therefore, the algorithm should work well for ERS-1 SAR images with a time interval of 3 days.

The results in Table 1 are plotted on a map see Fig. 9. Since neighbouring areas have similar mean drifts, for clearness an average value is used for the left part of the study area which includes several frames.

Since in the high Arctic area 70% of ice motion caused by wind (Thorndike and Colony, 1982), a comparison of two velocities (wind and ice motion) is shown in Fig. 10 where the wind dependence of ice motion can be observed from the corresponding velocity vectors. A quantity description of a relation for the two velocities can be obtained by a statistics analysis which will not be discussed in this paper.

7. DISCUSSION

In this paper a new correlation algorithm has been developed which derives motion information by matching entire scene of two images, instead individual features of the images. Two parameters, translation and rotation, are determined by the algorithm. These parameters are, then used to construct a motion field which is an accuracy measurement of the rigid motion of the ice pack. For non-rigid motion the method in this paper should be combined with other algorithms, e.g. the optical flow method (Verri, et al., 1990, and Sun, 1992). On the other hand the method developed here, could be modified to determine more parameters, e.g. scaling changes, rather than translation and rotation (Segman, 1992). All these parameters which describe the exact rate of co-ordinates deformation, such as vorticity, divergence and shear, are used to construct a high order motion field.

As manifested in Fig. 10, the first order motion information derived by the algorithm, will be useful for studying the wind dependence of ice motion. It may also be useful in other applications. Besides, the algorithm takes much less computation time than many other algorithms for the ice motion determination, and it could be used for a quick analysis of ice motion.

Table 1 - The image location is given by the centre co-ordinates of the reference image (early in time). The motion direction is defined by the angle from north to a motion vector. Positive angles are clockwise

Date	Frame number	Image location		Mean rotation	Mean drift (km)	Motion direction
		Latitude	Longitude			
20/9 - 20/9	1719	83.045°N	12.171°E	2°	28.3*	49.3°
26/9 - 29/9	1719	83.043°N	12.158°E	0°	28.3	- 128.2°
29/9 - 2/10	1719	83.045°N	12.167°E	0°	11.0	- 166.2°
20/9 - 26/9	1737	83.489°N	5.508°E	4°	30.1	51.7°
26/9 - 29/9	1737	83.489°N	5.494°E	0°	28.0	- 143.7°
29/9 - 2/10	1737	83.491°N	5.489°E	0°	12.5	166.7°
20/9 - 26/9	1755	83.838°N	- 2.007°E	3°	33.9	71.4°
26/9 - 29/9	1755	83.838°N	- 2.026°E	0°	29.8	- 146.1°
29/9 - 2/10	1755	83.840°N	- 2.029°E	0°	15.6	153.1°
20/9 - 21/9	1737 - 1755	83.489°N	5.508°E	- 1°	10.7	1.2°
21/9 - 24/9	1755	83.838°N	6.351°E	0°	31.3	47.4°
24/9 - 26/9	1755 - 1737	83.837°N	6.358°E	- 3°	12.3	- 170.2°
20/9 - 21/9	1755 - 1773	83.838°N	- 2.007°E	- 1°	11.1	- 1.8°
21/9 - 24/9	1773	84.073°N	- 1.897°E	0°	37.1	59.6°
24/9 - 26/9	1773 - 1755	84.072°N	- 1.891°E	- 2°	14.7	- 174.4 °
28/9 - 1/10	1683	81.932°N	14.631°E	0°	24.1	- 104.6°
1/10 - 4/10	1683	81.902°N	14.566°E	3°	18.1	178.3°
17/8 - 20/8	FD image	84.100°N	36.569°E	0°	23.4	- 10.1°
17/8 - 20/8	FD image	83.905°N	28.210°E	0°	20.2	- 15.1°

* The value derived from the sub-scene shown in fig. 8a and 8b

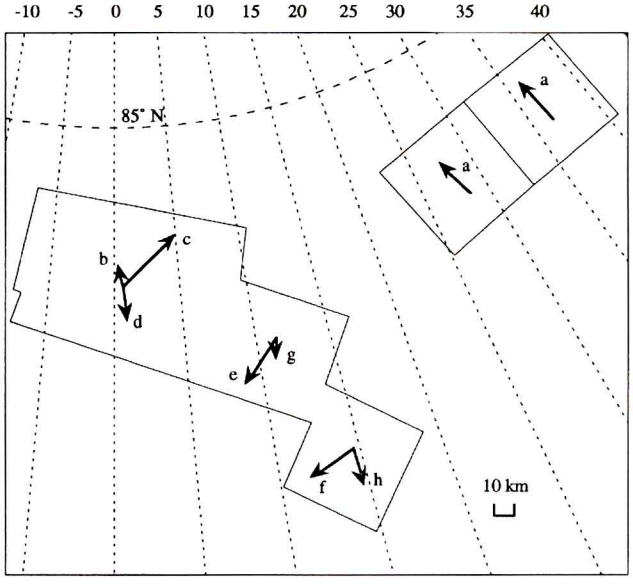

Fig. 9 - Mean drift plots, where the letters a - h indicate different time periods,
a: 17 to 20 August; b: 20 to 21 September; c: 21 to 24 September; d: 24 to 26 September; e: 26 to 29 September; f:28 September to 1 October; g: 29 September to 2 October; and h: 1 to 4 October

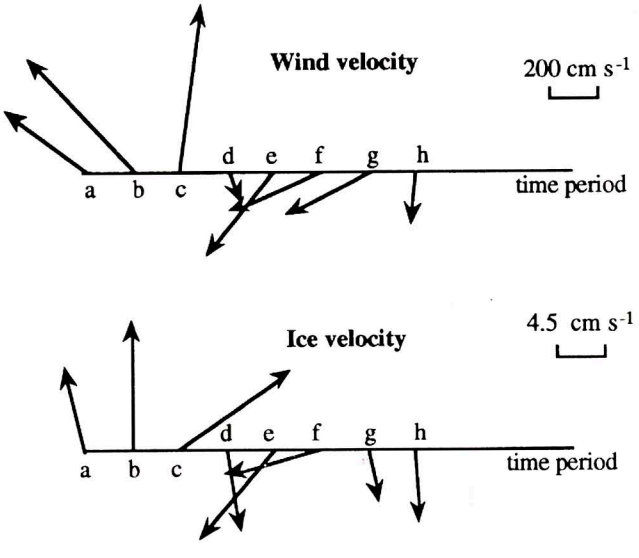

Fig. 10 - The temporal vector series of ice velocity and wind velocity, where the letters a - h indicate different time periods, a: 17 to 20 August; b: 20 to 21 September; c: 21 to 24 September; d: 24 to 26 September; e: 26 to 29 September; f:28 September to 1 October; g: 29 September to 2 October; and h: 1 to 4 October

ACKNOWLEDGEMENT

This work is supported by Swedish National Space Board.

REFERENCES

Castro E.D. & Morandi C., 1987, "Registration of translated and rotated images using finite Fourier transforms," IEEE Trans. Pattern Anal. Machine Intell., Vol. 6, pp. 700-703.

Banfield J., 1991, "Automated tracking of ice floes: A stochastic approach," IEEE Transaction on Geoscience and Remote Sensing, Vol. 29, No. 6, pp. 905-911.

Barry R.G., Serene M. C. & Maslanik J. A., 1993, "The ARCTIC sea ice-climate system: Observations and modelling," Reviews of Geophysics, 31, 4, pp 397-422.

Fily M. & Rothrock D. A., 1987, "Sea ice tracking by nested correlations," IEEE Trans. Geosci. Remote Sensing, Vol. GE-25 No. 5, pp. 570-580.

Lee D. J., Krile T. F. & Mitra S., 1988, "Power spectrum and spectrum techniques applied to image registration," Applied Optics, Vol. 27, No. 6, pp. 1099-1106.

McConnell R., Kwok R., Curlander J. C., Kober W. & Pang S.S., 1991, "Ψ-S Correlation and Dynamic time warping: Two methods for tracking ice floes in SAR images," IEEE Transaction on Geoscience and Remote Sensing, Vol. 29, No. 6, pp. 1004-1012.

Segman J., 1992, "Fourier cross correlation and invariance transformations for an optimal recognition of functions deformed by affine groups," J. Opt. Soc. Am. A, Vol. 9, No. 6, pp. 895-902.

Sun Y., 1992, "Ice motion retrieval form SAR imagery in terms of intensity derivative," Proceedings of IGARSS' 92 Symposium, Houston, Texas, U.S.A. May 1992, Vol. 1, pp. 585-587.

Thorndike, A. S., and Colony, R., 1982, "Sea ice motion in response to geostrophic winds, J. Geophys. Res., 87, pp. 5845-5852.

Vesecky J. F., Samadani R., Smith M. P., Daida J. M. & Bracewell R., 1987, Observing rotation and deformation of sea ice with SAR, Proceedings of IGARSS' 87 Symposium, New York: IEEE, pp. 1137-1146.

Vesecky J. F., Samadani R., Smith M. P. & Daida J. M., 1988, Observation of sea-ice dynamics using synthetic aperture radar images: Automated analysis, IEEE Transaction on Geoscience and Remote Sensing, Vol. 26, No. 1, pp. 38-47.

Verri A., Girosi F. & Torre V., 1990, "Differential techniques for optical flow," J. Opt. Soc. Am. A, Vol. 7, No. 5, pp. 912-922.